

RESEARCH

Open Access



# The formin FMNL2 plays a role in the response of melanoma cells to substrate stiffness

Joshua D. Clugston<sup>1</sup>, Sarah Fox<sup>2</sup>, James L. Harden<sup>1\*</sup> and John W. Copeland<sup>2\*</sup>

## Abstract

**Background** Cells constantly sense and respond to changes in their local environment to adapt their behaviour and morphology. These external stimuli include chemical and mechanical signals, and much recent work has revealed the complexity of the cellular response to changes in substrate stiffness. We investigated the effects of substrate stiffness on the morphology and motility of A2058 human melanoma cells. FMNL2, a formin protein associated with actin cytoskeleton dynamics, regulates melanoma cell morphology and motility, but its role in stiffness sensing remains unclear. This study examines how A2058 cells respond to substrates of varying stiffness and evaluates the impact of FMNL2 depletion on these responses.

**Results** We found that with increasing substrate stiffness the cells transitioned from a rounded cell morphology to progressively more elongated morphologies with a concomitant increase in actin stress fiber alignment. Depletion of FMNL2 expression amplified these morphological changes, with knockdown cells showing consistently greater elongation and more pronounced stress fiber alignment compared to controls. Notably, the orientational order parameter ( $S$ ) revealed higher alignment of actin filaments along the cell's long axis in knockdown cells. Substrate stiffness also affected cell motility, indicated by an apparent optimal stiffness that maximized motility followed by a notable decrease in distance travelled during migration on progressively stiffer substrates. This decrease was largely attributable to a decrease in the time the cells spent in motion as the substrate stiffness increased. FMNL2 depletion significantly exacerbated this effect, with knockdown cells traveling shorter net distances and spending less time moving across all substrates.

**Conclusions** This study demonstrates that substrate stiffness profoundly influences A2058 melanoma cell morphology and motility, with FMNL2 playing a pivotal regulatory role. Our observations suggest that FMNL2 is critical for maintaining motility and morphological adaptability under increased stiffness. Loss of FMNL2 enhanced stress fiber alignment and cell elongation while impairing motility, particularly on stiff substrates, revealing FMNL2 as a mechanosensitive effector. This work highlights the need to study metastatic cell behaviour on substrates with biologically relevant properties and provides the foundation for future effort to determine the mechanism by which FMNL2 participates in the melanoma cell response to substrate stiffness.

**Keywords** Cell motility, FMNL2, Melanoma, Substrate stiffness

\*Correspondence:  
James L. Harden  
jharden@uottawa.ca  
John W. Copeland  
jcopelan@uottawa.ca

<sup>1</sup>Department of Physics, Faculty of Science, University of Ottawa, STEM Complex, 150 Louis-Pasteur Private, Ottawa, ON K1N 6N5, Canada

<sup>2</sup>Department of Cellular and Molecular Medicine, Faculty of Medicine, University of Ottawa, 3155 Roger Guindon Hall, 451 Smyth Rd, Ottawa, ON K1H 8M5, Canada



© The Author(s) 2025. **Open Access** This article is licensed under a Creative Commons Attribution-NonCommercial-NoDerivatives 4.0 International License, which permits any non-commercial use, sharing, distribution and reproduction in any medium or format, as long as you give appropriate credit to the original author(s) and the source, provide a link to the Creative Commons licence, and indicate if you modified the licensed material. You do not have permission under this licence to share adapted material derived from this article or parts of it. The images or other third party material in this article are included in the article's Creative Commons licence, unless indicated otherwise in a credit line to the material. If material is not included in the article's Creative Commons licence and your intended use is not permitted by statutory regulation or exceeds the permitted use, you will need to obtain permission directly from the copyright holder. To view a copy of this licence, visit <http://creativecommons.org/licenses/by-nc-nd/4.0/>.

## Background

Directional cell migration is promoted by structural, chemical and physical signals that activate intracellular signaling pathways which govern cytoskeletal dynamics [1]. Indeed, the mechanical properties of the cellular microenvironment have a profound impact on many aspects of cell behaviour, affecting 2D and 3D cell migration as well as cell morphology [2, 3]. In vivo, cells encounter a range of mechanical environments and substrates with stiffnesses many orders of magnitude lower than the plastic or glass used in many in vitro studies. Mechanical signals such as substrate stiffness are sensed by actin-based structures that probe the surrounding environment during physiological and pathophysiological migratory events; directional migration in response to stiffness gradients is known as durotaxis [2].

Substrate stiffness is also directly linked to cell morphology, as cell area often increases on stiffer substrates due to the increased rate of focal adhesion (FA) formation [3–6]. Moreover, the formation of FAs is associated with the generation of tensile forces within the substrate, and the magnitude of these forces can change depending on the substrate stiffness [6–10]. This response is due, in part, to the cell's ability to exert variable traction forces, facilitating more significant interactions with the substrate and leading to increased FA formation [7–9]. Thus, cell motility is also linked to substrate stiffness, as the increased number of FAs increases their turnover rate, prolonging the cycle of attachment and detachment to the substrate [7, 8]. Mechanosensing is mediated by actin stress fibers which are anchored at focal adhesions and directly connect the cytoskeleton to the extracellular environment. Substrate stiffness has also been shown to affect the formation and organization of stress fibers. On rigid substrates, cells will often have well aligned stress fibers and focal adhesions along the major cell axis, while both stress fibers and focal adhesions become radially oriented on softer substrates [11, 12]. In addition to stress fibers, both finger-like filopodia, and flat, sheet-like lamellipodia, have been shown to be part of the cellular apparatus that detects substrate stiffness [2].

During migration, filopodia assist in guiding the cell by probing the environment and establishing connections with the substrate. These protrusions are dependent on formin proteins which directly regulate actin polymerization and the binding and bundling of F-actin [13–17]. Formin-like 2 (FMNL2) is a formin protein associated with filopodia assembly in multiple cell lines [16–18] and is required for filopodia assembly and normal cell motility in melanoma cells and other cancer cell lines [19–21]. Conversely, overexpression of FMNL2 is sufficient to induce filopodia assembly [17, 18, 22]. FMNL2 also contributes to lamellipodia formation and force generation at the leading edge in migrating melanoma cells [23].

Finally, FMNL2 has also been found to be necessary in the formation and turnover of cell-cell contacts, as well as cell-substrate adhesion sites [24, 25]. Thus, FMNL2 activity is involved in the assembly of multiple subcellular structures that are implicated in sensing the physical properties of the extracellular environment.

Despite the importance of the mechanical environment to metastatic cell behaviour, few studies have investigated the effects of substrate stiffness on melanoma cell migration and morphology [26]. To shed more light on the role of substrate stiffness in melanoma cell motility, we assessed the behaviour of A2058 human melanoma cells plated on fibronectin functionalized substrates with a range of biologically relevant elastic moduli. We found that A2058 cell morphology changed with increasing stiffness: the average cell area increased and more elongated cell morphologies with long, well-aligned stress fibers were observed. We also found that these cells exhibit a bimodal mode of cell motility, punctuated by alternating periods of motion and arrest. Notably, cell motility peaked on an elastic modulus of 0.5 kPa and the cells became progressively less motile on stiffer substrates, an effect attributable to a reduction in time spent moving on the stiffer substrates. We also studied the effect of silencing the protein FMNL2 in A2058 cells. The FMNL2 knockdown cells showed qualitatively similar behaviour, but they were less motile and more elongated than control cells on the same substrate. Depleting FMNL2 expression resulted in the cells spending less time in motion on the stiffer substrates than control cells, which resulted in a smaller average net distance travelled. Our results are consistent with recent reports that specific adherent cell-types become more elongated and less motile with increasing substrate stiffness, exhibiting negative durotaxis [26, 27]. Moreover, the results of our study indicate that the suppression of FMNL2 plays a significant role in modulating cell morphology and motility on substrates of different moduli, implying a potential role for FMNL2 in this process.

## Results

### Increasing substrate stiffness induces melanoma cell elongation

Cell proliferation, invasion, and speed have all been shown to change when cells are introduced into environments of different stiffness [2]. To gain insight into how the mechanical environment affects melanoma cell behaviour, we first characterized the effects of substrate stiffness on the morphology of adherent A2058 human melanoma cells. On extremely stiff substrates (>1 GPa), such as glass or tissue culture plastic, A2058 cells have a trapezoidal morphology and exhibit extensive stress fiber formation [17]. To test the effects of more physiologically relevant substrate stiffnesses on A2058 cell morphology

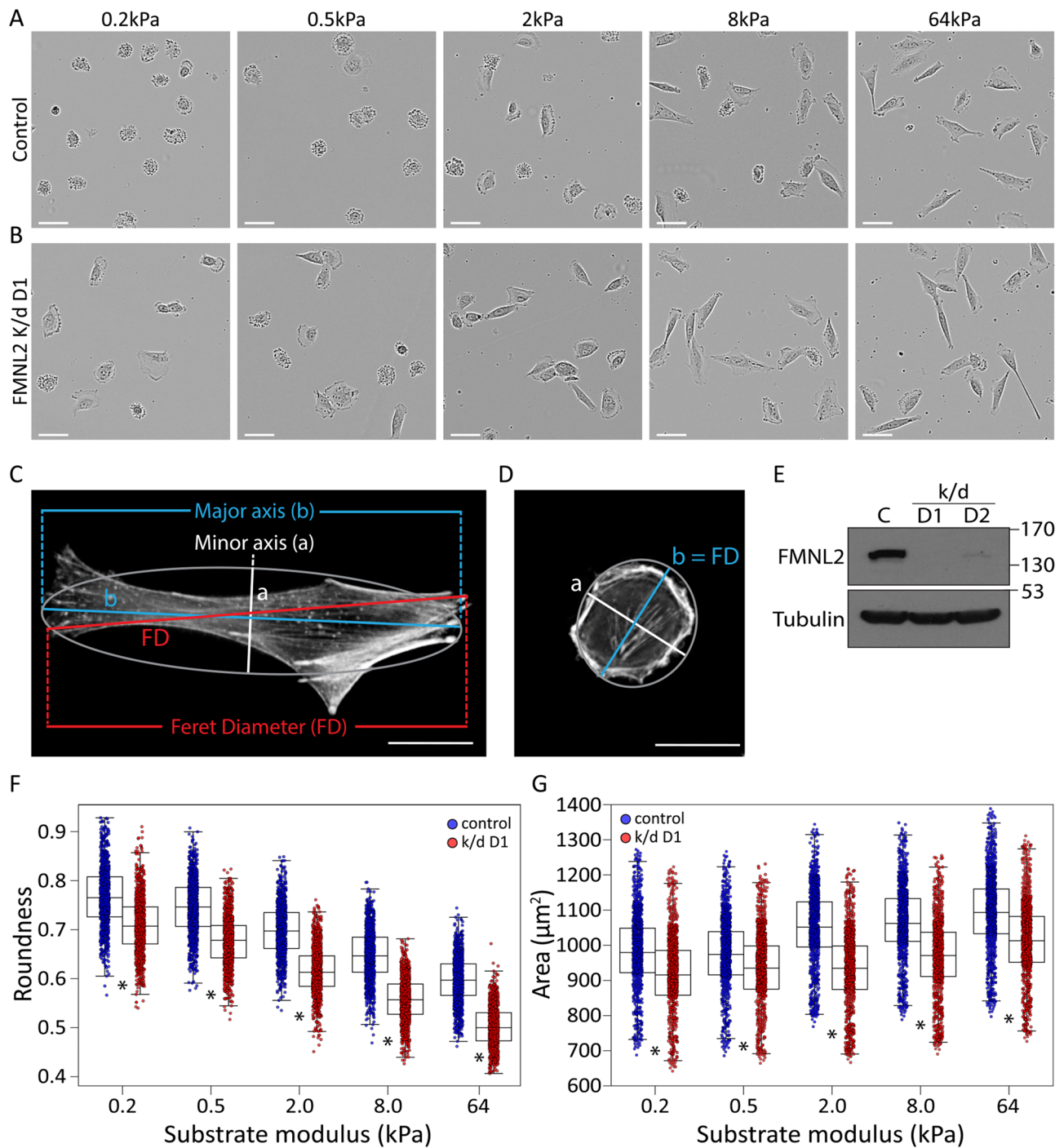
we employed substrates with a range of elastic moduli, and to assess a potential role for FMNL2 in this process, FMNL2 expression in these cells was knocked down using siRNA. Control and FMNL2-depleted A2058 cells were plated on fibronectin functionalized silicone gel substrates with moduli of 0.2 kPa, 0.5 kPa, 2.0 kPa, 8.0 kPa, and 64.0 kPa. On soft substrates (0.2 & 0.5 kPa), control cells adopted a more circular morphology. However, with increasing modulus (2, 8 & 64 kPa), the cells progressively became more elongated (Fig. 1A and Table 1). This behavior is reflected quantitatively by the average roundness value,  $R$ , which was found to decrease as the substrate modulus increased (Fig. 1F and Table 1).  $R$  for the control A2058 cells decreased from  $0.763 \pm 0.002$  on the 0.2 kPa substrate to  $0.615 \pm 0.001$  on the 64.0 kPa substrate. A similar trend was observed in the FMNL2 k/d cells (Fig. 1B,F Table 1), although these cells adopted more elongated conformations in comparison to the control cells for all elastic moduli, with  $R$  decreasing from  $0.714 \pm 0.002$  on the 0.2 kPa substrate to  $0.534 \pm 0.001$  on the 64.0 kPa substrate. An anti-FMNL2 immunoblot confirming the extent of FMNL2 knockdown by transient transfection of siRNA is shown in Fig. 1E. Duplex D1 was consistently more effective in FMNL2 depletion than duplex D2. Nevertheless, similar results were obtained in FMNL2 k/d cells using the second siRNA duplex (D2) (Supplemental Figure S1 and Table S1).

Comparing the  $R$  values for the control and knockdown cells on equivalent substrates (Table 1, Supplemental Table S1), we can see that their difference,  $\delta R = R_{kd} - R_c$ , was consistently negative, indicating that the knockdown cells adopted more elongated morphologies than their control counterparts. The cell area ( $A$ ), perimeter ( $P$ ), and Feret diameter ( $FD$ ), defined as the longest distance between two points along an object's boundary (Fig. 1C, D), were also calculated for each cell and averaged over the cell population to further characterize the effect of substrate stiffness on cell morphology. All values were found to monotonically increase with increasing substrate stiffness (Fig. 1G, Table 1). For additional insight, we examined the net average change of these parameters ( $\Delta A$ ,  $\Delta P$ ,  $\Delta FD$ , and  $\Delta R$ ) relative to their values on the softest substrate (0.2 kPa) (Supplemental Table S3). For instance, the net average area increase,  $\Delta A$ , between the 0.2 kPa substrate and the 64.0 kPa substrate was  $\Delta A = 129 \pm 11 \mu\text{m}^2$  for the native A2058 cells and  $\Delta A = 107 \pm 9 \mu\text{m}^2$  for the FMNL2 k/d cells. Likewise, the net average cell perimeter and Feret diameter increases between the 0.2 kPa and 64.0 kPa substrates, with  $\Delta P = 30.1 \pm 1.1 \mu\text{m}$  and  $\Delta FD = 14 \pm 0.3 \mu\text{m}$  for the control cells and with  $\Delta P = 32.4 \pm 1.1 \mu\text{m}$  and  $\Delta FD = 14.2 \pm 0.2 \mu\text{m}$  for the FMNL2 k/d cells (Supplemental Table S3). This increase in area and perimeter indicates that the control cells were more spread as the substrate stiffness

increased, while the increase in Feret diameter shows that these cells also became more elongated with increasing stiffness (Fig. 1A, B). Notably, when compared to the control A2058 cells, FMNL2 k/d cells showed smaller values of average cell area ( $A$ ), and larger values for average cell perimeter ( $P$ ) and Feret diameter ( $FD$ ) on equivalent stiffness substrates, consistent with their greater elongation. Supplemental Table S2 reports the differences ( $\delta A$ ,  $\delta P$ ,  $\delta FD$ , and  $\delta R$ ) between values of  $A$ ,  $P$ ,  $FD$ , and  $R$  for FMNL2 k/d cells relative to the control cells. The observation of negative  $\delta A$  and positive  $\delta P$  and  $\delta FD$  for different modulus substrates further corroborates the negative relative average roundness  $\delta R$  results, as these changes indicate that the knockdown cells became more elongated than the control cells on the same substrate. Similar results were obtained in FMNL2 k/d cells using a second siRNA duplex (D2) (Supplemental Tables S1, S2, S4).

#### Decreased substrate stiffness decreases actin fiber alignment

To further assess the changes in cell morphology, control and FMNL2 k/d cells plated on substrates of increasing stiffness were fixed and stained with phalloidin to image filamentous actin. The orientation and structure of the actin fibers were notably different between the soft and stiff substrates in both control and knockdown cells (Fig. 2). As the substrate stiffness increased, the angular orientation of the fibers became more tightly distributed around  $0^\circ$ , i.e. parallel to the direction of the Feret diameter (Fig. 2B). Moreover, on both soft and stiff substrates, the angular distribution of the knockdown cell fibers was also more tightly distributed around  $0^\circ$  in comparison to control cells (Fig. 2B). To further quantify this effect, we defined a 2D orientational order parameter ( $S$ ), which quantifies the alignment of the actin fibers within the cell with respect to a defined axis - the direction of the cell elongation as given by the Feret diameter (Fig. 2C). This value can vary between  $-1$  and  $1$ , with values close to  $0$  indicating random orientation, values close to  $1$  showing preferential alignment of the stress fibers within the cell along the Feret diameter, and values close to  $-1$  indicating alignment perpendicular to the Feret diameter. As the substrate modulus increased, we found that  $S$  for both the control and knockdown cells increased with substrate modulus (Fig. 2E). Furthermore, there was a noticeable enhancement of  $S$  in the knockdown cells relative to the control cells. The values of  $S$  and the width of the distributions of fiber orientation both indicate that the actin fibers in the FMNL2 k/d cells were consistently more aligned with the long axis of the cell in comparison to the control cells. An anti-FMNL2 immunoblot confirming the extent of FMNL2 knockdown is shown in Fig. 2D. Similar results were obtained with knockdown of FMNL2 using a second siRNA duplex (Supplemental Figure S2).

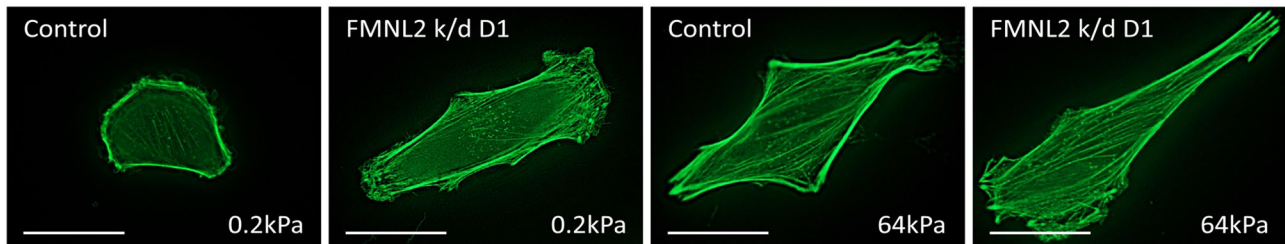
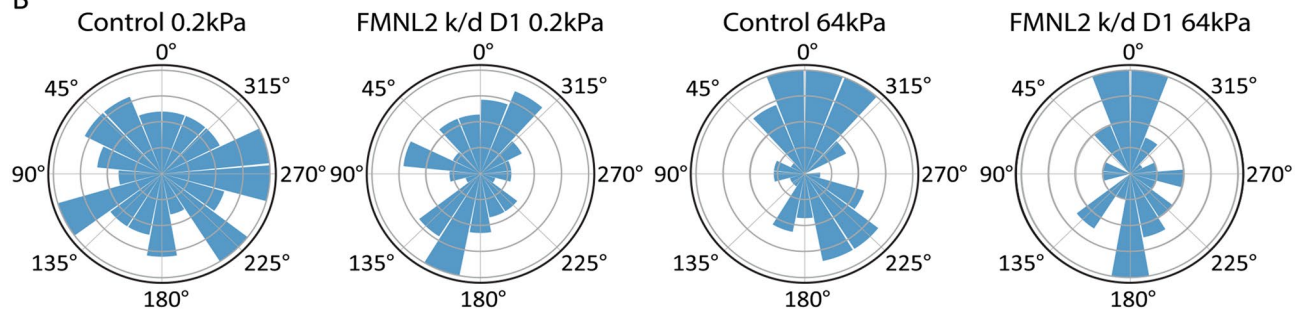
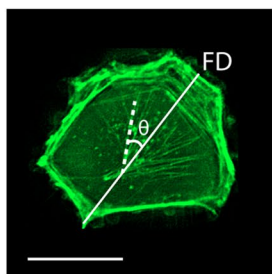
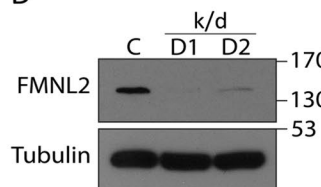
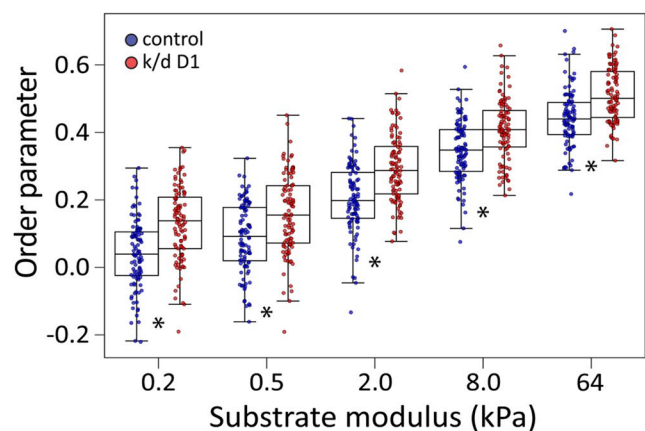


**Fig. 1** A2058 Morphology Changes Across Substrates with Increasing Modulus. **A** Representative phase contrast images of control A2058 cells plated on substrates with the indicated elastic moduli. **B** Representative phase contrast images of FMNL2-depleted A2058 cells plated on substrates with the indicated moduli. Scale bar = 25  $\mu\text{m}$ . **c, d** Representative images of an elongated (**C**) and round (**D**) cell showing the minor and major axis with the ellipse fit to each cell. The Feret Diameter (FD), the largest distance between points around the perimeter of the cell, is also shown. Scale bar = 20  $\mu\text{m}$ . **E** Anti-FMNL2 immunoblot confirming the extent of FMNL2 knockdown by transient transfection of siRNA. Duplex D1 was consistently more effective in FMNL2 depletion than duplex D2. Tubulin was used as a loading control. **F** The average roundness value  $R$  for control and FMNL2 knockdown cells across all substrates (see Table 1 for all cell morphology parameter values). **G** The average area value for control and FMNL2 knockdown cells across all substrates.  $N=3$ , with approximately  $n=1500$  cells analyzed per substrate.  $*p < 0.0001$

**Table 1** Morphological changes in A2058 cells on increasing moduli substrates for control and FMNL2 depleted cells

Modulus (kPa)	Control				k/d D1			
	A ( $\mu\text{m}^2$ )	P ( $\mu\text{m}$ )	FD ( $\mu\text{m}$ )	R	A ( $\mu\text{m}^2$ )	P ( $\mu\text{m}$ )	FD ( $\mu\text{m}$ )	R
0.2	951 $\pm$ 8	144.9 $\pm$ 0.8	44.1 $\pm$ 0.2	0.763 $\pm$ 0.002	897 $\pm$ 7	149.5 $\pm$ 0.8	46.7 $\pm$ 0.1	0.714 $\pm$ 0.002
0.5	947 $\pm$ 9	143.7 $\pm$ 0.7	44.2 $\pm$ 0.2	0.742 $\pm$ 0.002	910 $\pm$ 6	150.4 $\pm$ 0.9	47.5 $\pm$ 0.1	0.683 $\pm$ 0.002
2.0	1030 $\pm$ 8	154.7 $\pm$ 0.7	47.5 $\pm$ 0.1	0.704 $\pm$ 0.001	923 $\pm$ 7	158.3 $\pm$ 0.8	50.6 $\pm$ 0.2	0.633 $\pm$ 0.001
8.0	1050 $\pm$ 8	165 $\pm$ 0.8	52.9 $\pm$ 0.1	0.663 $\pm$ 0.001	961 $\pm$ 6	171.3 $\pm$ 0.9	55.8 $\pm$ 0.2	0.583 $\pm$ 0.001

Values for the average area (A), perimeter (P), Feret diameter (FD), and Roundness (R) are shown for the control and knockdown (siRNA duplex D1) cells on each substrate. The error on each value is the standard error of the mean. N=3, with approximately 1500 cells analyzed per table value

**A****B****C****D****E**

**Fig. 2** Substrate modulus affects actin stress fiber orientation in A2058 cells. **A** Representative images of the cells analyzed in **E** for control and FMNL2 depleted cells plated on the indicated substrates. Cells were fixed and stained with phalloidin to visualize actin filaments. Scale bar = 20  $\mu\text{m}$ . **B** Windrose plots showing the orientation of the actin fibers with respect to the cells' Feret diameter for control and FMNL2 depleted cells plated on 0.2 kPa and 64 kPa substrates. Increases in substrate modulus and FMNL2 depletion both yield a tighter distribution around 0, indicating increased filament alignment. **C** An annotated image of a cell with a white bar showing the Feret diameter (FD), with the angle  $\theta$  being the angle between the FD and an actin fiber shown with the dashed line.  $\theta$  is then used to calculate the 2D orientational order parameter (S). **D** Anti-FMNL2 immunoblot confirming the extent of FMNL2 knockdown by transient transfection of siRNA. Tubulin was used as a loading control. **E** 2D orientational order parameter S quantifying average orientation of F-actin with respect to the cell Feret diameter. Increasing substrate stiffness increases the 2D order parameter. N=3, with approximately 100 cells analyzed per cell type and substrate. \* $p < 0.0001$

### Increasing substrate modulus decreases cell motility

To gain further insight into the effects of substrate stiffness on cell behaviour, A2058 cells were tracked for 24 h to compare cell motility across the different substrates. These cells exhibited a bimodal pattern of cell motility characterized by alternating periods of motion and arrest. Overall, for both control and FMNL2 k/d A2058 cells, the average net distance travelled,  $\bar{D}$ , decreased with increasing substrate modulus (Fig. 3 and Supplemental Table S5). We also calculated the difference in the average net distance traveled ( $\Delta\bar{D}$ ) between the 0.2 kPa

substrate and each subsequent stiffness substrate for both the control and knockdown cell populations (Supplemental Table S6). The difference in  $\Delta\bar{D}$  between the softest substrates (0.5–0.2 kPa) was insignificant, whereas all other comparisons showed significant decreases. Additionally,  $\Delta\bar{D}$  was consistently negative, further highlighting the monotonic decrease in  $\bar{D}$  for both cell types as substrate stiffness increased. Furthermore, across all five substrates tested, the knockdown cells consistently travelled an average net distance  $\delta\bar{D}$  between  $39 \pm 3 \mu\text{m}$  and  $55 \pm 4 \mu\text{m}$  less than the control cells (Supplemental Table

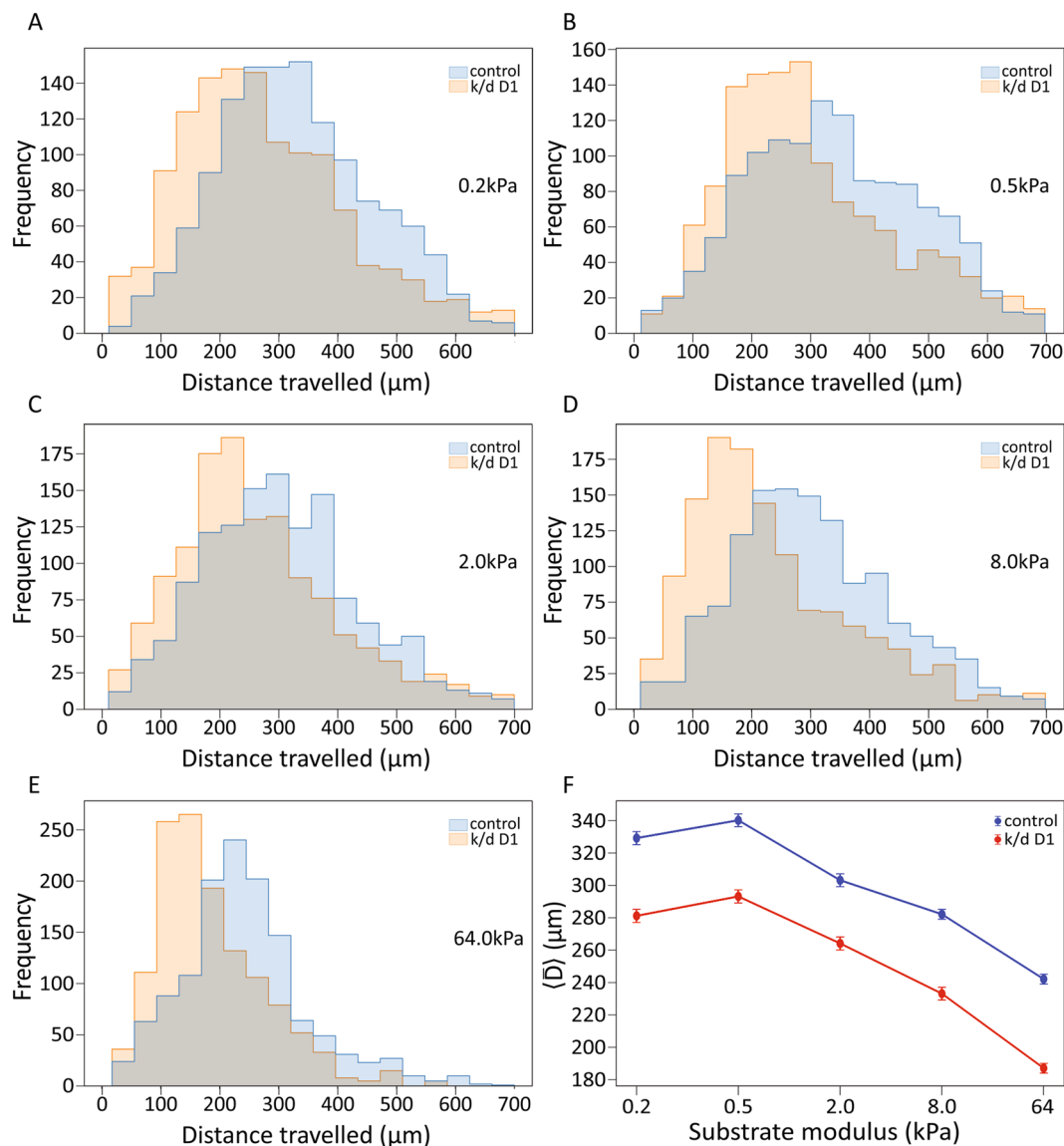


**Fig. 3** Cell motility is decreased with increased modulus. (A–E) Histograms of the net distance  $D$  travelled across all substrates for control (blue) and FMNL2 knockdown (orange) A2058 cells, with the overlap region shown in gray. Knockdown cells show a smaller average distance travelled than control cells as indicated by the shift in the histogram. Values are derived from cells tracked by live-cell imaging from the experiments shown in Fig. 1F. A line graph showing the average distance travelled for all control and knockdown cells with increasing substrate stiffness. The error bars are the SEM.  $N = 3$ , with approximately 1000 cells analyzed per substrate

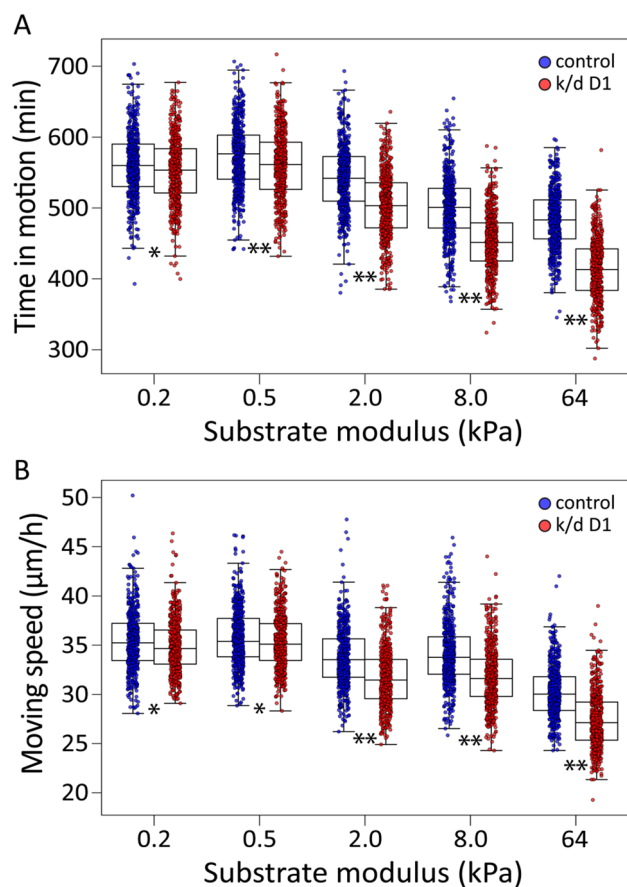


**Fig. 4** Time spent in motion and moving speed for control and FMNL2 knockdown cells. **A, B** Boxplots showing the time spent moving **A** and the moving speed **B** for control (blue) and FMNL2 knockdown (red) cells with increasing substrate modulus. Increasing stiffness resulted in decreased time in motion and moving speed. FMNL2 depleted cells spent less time in motion than control cells on each substrate.  $N=3$ , with approximately 1000 cells analyzed per substrate and cell type. \* $p < 0.05$ , \*\* $p < 0.0001$

S5). This is clearly observed in the shift in distribution of distance  $D$  travelled for the knockdown cells towards a smaller average value across all substrates (Fig. 3A-E).

Decreased distance travelled may result from either decreased cell speed or less time spent in motion. To distinguish between these possibilities, and to characterize the punctuated cell motility observed for A2058 cells, we next examined the ensemble-averaged time spent moving by the cells,  $t_m$ , and its dependence on substrate stiffness. The ensemble-averaged cell speed  $s_m$  was also calculated

using  $t_m$  and  $\bar{D}$  and correlated with substrate modulus. This comparison can determine whether cell motility is intrinsically slower on stiffer substrates, or if cells spend progressively less time moving on substrates of increasing stiffness. It also more clearly assesses the underlying differences in motility between the control and knockdown cells. The average time in motion  $t_m$  for both control and FMNL2 k/d cells increased slightly from the 0.2 kPa to the 0.5 kPa modulus substrates, before monotonically

diminishing with increasing substrate stiffness above 0.5 kPa (Fig. 4A and Supplemental Table S7). Moreover, the average cell moving speed  $s_m$  followed these same trends with increasing stiffness (Fig. 4B and Supplemental Table S8) for both groups, but in a less drastic manner. Interestingly, FMNL2 k/d cells spent significantly less time in motion than the control cells on the 2.0 kPa, 8.0 kPa, and 64.0 kPa substrates. In contrast, the difference in time in motion ( $\delta t_m$ ) between control and knockdown cells was much smaller on the 0.2 kPa and 0.5 kPa substrates, as shown in Supplemental Table S7. Comparing the average moving speed  $s_m$  between the two cell types on equivalent substrates, the knockdown cells moved more slowly than the control A2058 cells, but the differences, as shown by  $\delta s_m$  (Supplemental Table S8), are less pronounced than those seen in the time spent moving,  $t_m$ . We also calculated the difference in time in motion ( $\Delta t_m$ ) and average moving speed ( $\Delta s_m$ ) between the 0.2 kPa substrate and each subsequent stiffness substrate for both the control and knockdown cell populations (Supplemental Table S6). Interestingly,  $\Delta t_m$  between the softest substrates (0.5–0.2 kPa) indicated a modest but significant increase in time spent in motion, whereas all other comparisons showed significant decreases. Depletion of FMNL2 expression with a second siRNA duplex produced similar results (Supplemental Figures S3–S4 and Tables S5–S8). Overall, the decrease in the average distance travelled with increasing substrate modulus is largely attributable to the decreased time spent in motion by both control and knockdown cells, with a smaller contribution from their decreased average speed, and FMNL2 k/d cells moved systematically shorter distances and spent less time in motion than control A2058 cells on equivalent substrates.

## Discussion

In this study, we tested the effects of substrate stiffness on the morphology and motility of A2058 human melanoma cells. On the softest substrates, the cells consistently adopted circular morphologies and as the substrate stiffness increased, they became progressively more elongated. This effect was quantified by the cell roundness parameter  $R$  which confirmed the impact of substrate stiffness on cell shape. The increase in elongation (decrease in  $R$ ) was matched by an increase in the average area  $A$ , perimeter  $P$  and Feret diameter  $FD$  of each cell, consistent with the cells becoming more elongated and more spread as the substrate became stiffer. Similarly, the increase in elongation on stiffer substrates was accompanied by an increase in stress fiber formation and stress fiber alignment as quantified by the rising fiber orientational order parameter  $S$ . Knockdown of FMNL2 expression diminished the increase in cell area induced with increasing substrate stiffness relative to the control

cells. FMNL2 depletion was also associated with a concomitant increase in cell elongation and actin filament alignment.

Cell motility is driven by forces generated by the actin network pushing against the lamellipodial membrane at the leading edge and by traction forces generated by integrin adhesion complexes (IAC). Molecular clutch theory suggests that cells move toward regions where the highest force is exerted. In positive durotaxis, higher force is generated on stiffer substrates and is dependent on the focal adhesion protein Talin acting as part of the IAC mechanosensory apparatus. In other cases, cells migrate toward an optimal stiffness determined by the substrate modulus and the cytoskeletal regulatory machinery [2]. In such cases, negative durotaxis may occur, in which cells migrate towards softer substrates where an optimal stiffness generates maximum force. Indeed, we found that A2058 cells exhibited two distinct motility regimes: an initial regime where cell motility first increased modestly with increasing elastic modulus below 0.5 kPa, followed by a second regime where cells became substantially less motile with further increase of elastic modulus. We also note a correlation between the substrate induced changes in cell roundness and motility in A2058 cells in both regimes. On the softer substrates ( $\leq 0.5$  kPa), cells exhibited a rounder morphology and enhanced motility, while on stiffer substrates cells became progressively elongated and exhibited diminishing motility with increasing modulus, suggesting the existence of an optimal stiffness for the migration of these cells near an elastic modulus of 0.5 kPa. The behaviour observed for A2058 cells on the softer substrates is consistent with previous reports of cells that undergo positive durotaxis [11, 12]. In contrast, on stiffer substrates the changes in A2058 cell motility with increasing modulus are more consistent with cells that exhibit negative durotaxis [2, 27]. Further analysis revealed that with increasing substrate stiffness above 0.5 kPa, the decrease in cell motility was largely attributable to a substantial decrease in the average time in motion of the cells, with the concomitant decrease in average speed while in motion playing a relatively minor role. As with the effects on cell morphology, FMNL2 depletion also inhibited cell motility across all substrates with a greater effect on stiffer substrates (2.0, 8.0 and 64 kPa). As with wild-type A2058 cells, the decrease in the motility of the FMNL2 knockdown cells was largely due to the decrease in the average time in motion of the cells with increasing substrate modulus, possibly providing clues to the biological origins of this motility inhibition.

FMNL2 plays an important role in facilitating melanoma cell motility [18, 22, 28] and we found the FMNL2 knockdown inhibited cell migration on all substrates tested. This effect was significantly more pronounced on the stiffer substrates suggesting that the function of

FMNL2 in cell motility is governed by substrate stiffness. FMNL2 knockdown also had a significant effect on the stiffness induced changes in morphology. The knockdown cells were more elongated and had appreciably more stress fibers aligned with the long axis of the cell. Enhanced stress fiber alignment was somewhat unexpected given the association of formins with the assembly of these structures [29]. Similar results were obtained, however, following the depletion of the related protein FMNL1 in other cell-types [30] suggesting this might reflect the function of the FMNL formin subfamily in the regulation of actin dynamics. Indeed, FMNL2 activity is more closely associated with filopodia formation [13–18, 31] or with force generation at lamellipodia [22, 23]. FMNL2 is also found in the focal adhesion proteome of melanoma cells [32]. Lamellipodia, filopodia and focal adhesions have all been previously suggested to act as part of the mechanosensory apparatus [2, 33]. In this case, is FMNL2 part of the mechanosensing machinery acting either at filopodia, lamellipodia or the IAC, or is it a downstream effector that is regulated by mechanosignaling? Our results do not distinguish between these alternatives, although we note a recent study highlighted an effector role for FMNL3 in filopodia-based **positive** durotaxis in fibroblasts [34]. Similarly, our results are consistent with a model where FMNL2 acts as a mechanosensitive effector in **negative** durotaxis, given its more modest effects on cell behaviour on the softest substrates. Together these findings may suggest a general role for FMNL proteins in the cellular response to substrate stiffness.

## Conclusions

We found that increasing substrate stiffness above a characteristic value (near 0.5 kPa) had a marked effect on the morphology and motility of A2058 melanoma cells. These cells were observed to become more elongated, travel shorter distances, and spend less time in motion as the substrate modulus increased, behaviour consistent with cells that undergo negative durotaxis. In contrast, cell motility was somewhat enhanced with increasing stiffness below 0.5 kPa, consistent with an optimal substrate modulus near 0.5 kPa and positive durotaxis below this value. Interestingly, cell migration was inhibited in FMNL2 knockdown cells in comparison to control cells on the same substrates, indicating systematic quantitative differences between control and knockdown cells. These findings suggest that FMNL2 plays an important role in the pathways governing the response of A2058 cells to their extracellular environment, highlight the significant impact of substrate stiffness on A2058 cell behavior, and underlines the importance of using biologically relevant substrates for the assessment of metastatic cell behaviour.

## Methods

### Cell culture

A2058 (CRL-11147) melanoma cells obtained from the American Type Culture Collection were cultured in Dulbecco's modified Eagle's medium (Wisent; 319–007 CL) supplemented 10% v/v with fetal bovine serum (Wisent; 090–150-FBS) in 5% CO<sub>2</sub> according to the supplied guidelines. Mycoplasma contamination was tested biweekly.

Advanced Biomatrix CytoSoft® 6-well Plates– discovery kit #5190: Eppendorf 6-well cell culture plate (Eppendorf 0030.720.113) with a 0.5 mm layer of activated biocompatible silicone of defined elastic modulus were used for all live-cell imaging. Advanced Biomatrix CytoSoft® Imaging 24-well Plate 0.2 kPa (#5183) and 64 kPa (#5189): Eppendorf 24 well cell imaging plate (0030.741.021) #1.5 glass bottom with a ~0.03 mm layer of activated biocompatible silicone of defined elastic modulus were used for fixed cell imaging. Silicone surfaces were coated with a Fibronectin solution (bovine plasma, Sigma; F1141) at a final concentration of 10 µg/ml in DPBS (Wisent; 311–425 CL) for 1 h at room temperature. The fibronectin solution was removed, and the plates maintained in DPBS until the cells were added.

siRNA-mediated knockdown was performed as previously described [17] using Dharmafect1 (Horizon Discovery Ltd; T-2001-03) and the following siRNA duplexes: FMNL2 siRNA Duplex1 (IDT; hs.Ri.FMNL2.13.1); FMNL2 siRNA duplex2 (IDT; hs.Ri.FMNL2.13.2).

### Microscopy

Live cell imaging was performed on an Incucyte® S3 Live-Cell Analysis System (Sartorius). Full technical specifications can be found here: <https://www.sartorius.com/download/930502/incucyte-s3-technical-specification-sheet-8000-0527-c00-en-%96s-1%96data.pdf>. High-definition phase-contrast images were acquired using the 10X/NA 0.3 objective with an image resolution of 1.2 µm/pixel. 72 h after transfection with control or FMNL2 siRNA duplex, A2058 cells were seeded at a density of 60,000 cells per well in CytoSoft® 6-well Plates (Advanced Biomatrix – discovery kit #5190) with the indicated moduli ranging from 0.2 kPa to 64 kPa. Remaining cells were transferred to fresh 3.5 cm dishes and incubated at 37 °C, 5% CO<sub>2</sub>. Cells were imaged using the Incucyte® S3 Live-Cell Analysis System at 37 °C in a 5% CO<sub>2</sub> incubator. Phase contrast images were collected every 20 min for 24 h, the first time point at 2.5 h post seeding. Cells were then fixed for 10 min with freshly prepared 4% paraformaldehyde in PHEM (PIPES, Hepes, EGTA, MgCl<sub>2</sub>) for additional analysis [35]. The parallel cell samples were harvested and boiled in 1X Laemmli buffer to assess knockdown efficiency by immunoblotting.

High resolution fixed cell images were acquired using a Zeiss Axio Observer 7 inverted microscope with linear encoded stage and HXP 120 V light source with built in power supply, shutter, lamp module and infra-red filter. Zeiss filter set 37 Ex. BP 450/50 FT:480 Em. BP 510/50, 63 × 1.4NA oil immersion Plan-apochromat objective, detection with a Hamamatsu ORCA-Flash LT 16bit camera. Z-stacks captured with Zeiss Zen 3.0 software. 55 h after transfection with control or FMNL2 siRNA duplex, A2058 cells were seeded at a density of 2, 250 cells per well in CytoSoft® Imaging 24-well plates 0.2 kPa and 64 kPa moduli and incubated at 37 °C, 5% CO<sub>2</sub>. Remaining cells were transferred to fresh 3.5 cm dishes and incubated at 37 °C, 5% CO<sub>2</sub>. 72 h post transfection, cells were fixed for 10 min with freshly prepared 4% paraformaldehyde in PHEM (PIPES, Hepes, EGTA, MgCl<sub>2</sub>) [35]. The parallel cell samples were harvested in 1X Laemmli buffer and assessed for knockdown efficiency by immunoblotting.

### Immunofluorescence

Immunofluorescence was performed as in [17]. Briefly, cells fixed in 4% formaldehyde/PHEM buffer were permeabilized and blocked for 20 min in 0.3% Triton X-100, 5% donkey serum in 1×PBS, washed in 1×PBS, and incubated with Alexa Fluor 488 Phalloidin (Molecular Probes; A12379) diluted 1:200 in 0.03% Triton X-100 and 5% donkey serum in 1×PBS for 1 h at room temperature. Washed and stored in 1X PBS.

### Immunoblotting

siRNA knockdown efficiency was assessed by immunoblotting. Cells were washed with 1XPBS and harvested in 1x Laemmli buffer. Lysates were subjected to SDS-PAGE and immunoblotted with the indicated antibodies. Chemiluminescence was used for detection using the Immobilon® Crescendo western HRP substrate reagent (Millipore Sigma). FMNL2 was detected using chicken anti-FMNL2 [18] and Peroxidase AffiniPure™ Donkey Anti-Chicken IgY (IgG) (H+L) (Jackson ImmunoResearch Laboratories); tubulin with mouse anti-α-tubulin (Sigma; T5168) and Peroxidase AffiniPure™ Donkey Anti-Mouse IgG (H+L) (Jackson ImmunoResearch Laboratories).

### Statistical and error analysis

All experimental measurements were recorded, and the mean and standard deviation (SD) of these values were calculated. The uncertainty associated with each mean value was calculated using the standard error of the mean (SEM). For calculating the uncertainty on measurements using the calculated mean values, propagation of error was used to determine their associated error. To determine statistical significance between two measured

values, Analysis of Variance (ANOVA) testing was performed to discern any statistically significant differences between the groups. Tukey's post hoc analysis was then performed to identify significant results between the mean values of different groups. All statistical analyses were conducted with a pre-established alpha level of 0.05, denoting the threshold for statistical significance.

### Morphology and motility analysis

Using the Python package OpenCV, the tiff stacks were first thresholded, a process where the pixels are binarized based on their intensity, with pixels having a value less/greater than the defined threshold assigned to white (0)/black (1). The tiff stacks were subsequently filtered using a Gaussian blur to reduce noise in the image. To quantify the morphology of cells, the cells were first located using the OpenCV function "findContours", which identifies the boundary of objects in binarized images by looking for sharp increases or decreases in adjacent pixel values. Following this, the function "fitEllipse" was then used to fit an ellipse to the contours identified in the previous step. Using the contours, a mask was then created by converting all the pixels populating the inside of the contour into a binary image. The major and minor axis of the ellipse were then extracted and exported to a csv file, as well as the area, perimeter, and spatial coordinates of the boundary of the mask. With these values, we calculated the roundness of each cell ( $r_i$ ) as the ratio of the minor to major axis length of the fitted ellipse. We then averaged over all  $N$  cells on the substrate to obtain the group average roundness,

$$R = \langle r_i \rangle = \frac{1}{N} \sum_{i=1}^N r_i$$

To calculate the Feret diameter, a custom Python script calculated the distance between all points around the boundary of the mask, and then extracted the maximum value.

To track the cells, they were located using OpenCV's contour finding function, and then tracked for the entire tiff stack with the Discriminative Correlation Filter with Channel and Spatial Reliability (CSRT) tracker in OpenCV. This object tracking algorithm works by applying discriminative correlation filters to different feature channels of the image (color, texture, etc) to determine their reliability. Each channel is weighted independently of the others based on its assigned reliability, which the CSRT tracker assesses by measuring each channel's consistency in response over time, focusing on signal-to-noise ratio (SNR) to emphasize stable features and suppress noise. The tracker also learns to discriminate between the object and its background to enhance

accuracy when the background may contain distracting elements. At each time point, the position of each cell along the  $x$  and  $y$  axes were then recorded and exported as a csv file and analyzed to determine all motility measurements once tracking was complete. The net distance travelled by each cell was then calculated by summing the distance travelled between each time step  $\Delta t$  from an initial time  $t_0$  up to the total time  $T$ :

$$D = \sum_{t=t_0}^T d_t = \sqrt{(x(t + \Delta t) - x(t))^2 + (y(t + \Delta t) - y(t))^2}$$

The speed of each cell between each time step was also calculated to determine if the cell was moving. If the speed of the cell was  $<5 \mu\text{m/h}$ , then it was classified as not moving, as speeds less than this were often due to morphological changes in the cell that changed its center of mass, and not true movement. The time spent stationary and the time spent moving were then calculated for each cell using this restriction. These were averaged over the cell population to determine an ensemble-averaged moving time  $t_m$ . Likewise, the ensemble-averaged speed  $s_m$  was determined by averaging the mean cell speed during a cell trajectory over the cell population.

### Actin fiber analysis

For actin fiber alignment analysis, images were first preprocessed in ImageJ by enhancing the contrast of the image by 0.35%. Subsequently, the stack was then exported as a maximum projection intensity image. A binary mask was also created and exported by thresholding the image to separate the cell from the background. The analysis was then performed with a previously used method known as Alignment by Fourier Transform [36] with some modifications to their python scripts. This method segments the windows of a defined size, performs a fast Fourier transform on each window in the image, and then outputs a vector field representing the alignment of F-actin fibers in a cell. The orientation angle  $\theta$  for each fibre vector with respect to a central reference vector oriented along the major axis of the cell is then calculated and used to obtain a local F-actin orientational order parameter in a given cell [37]

$$s_{Local} = 2\cos^2\theta - 1$$

This value characterizes the orientation of a given F-actin fibre with respect to the major axis of the cell. These local fibre order parameters are then averaged over all fibres in their cell to obtain the orientational order parameter of the entire cell:  $S_C = \langle S_{Local} \rangle$ . We can then average over all the cells on a given substrate to obtain the global orientational order parameter:  $S = \langle S_C \rangle$ .

## Supplementary Information

The online version contains supplementary material available at <https://doi.org/10.1186/s12860-025-00538-8>.

Supplementary Material 1

Supplementary Material 2

Supplementary Material 3

## Acknowledgements

The authors acknowledge the outstanding support of the Cell Biology and Image Acquisition Core (RRID: SCR\_021845) at the University of Ottawa, Faculty of Medicine.

## Authors contributions

JC, JLH and JWC designed the study. JC and SF performed the experiments and prepared the figures. JC analyzed the data and was the major contributor in writing the manuscript. JLH and JWC supervised the research project. All authors read and approved the final manuscript.

## Funding

This research was funded by CIHR Project Grant PJT 183776 awarded to JWC and by NSERC Discovery Grant RGPIN-2024-06902 awarded to JLH.

## Data availability

The authors declare that the data supporting the findings of this study are available within the paper and its Supplementary Information files. Raw image data files of microscopy experiments are available from the corresponding author upon reasonable request.

## Declarations

### Ethics approval and consent to participate

Not applicable.

### Consent for publication

Not applicable.

### Competing interests

The authors declare no competing interests.

Received: 2 December 2024 / Accepted: 4 April 2025

Published online: 29 April 2025

## References

- Sengupta S, Parent AC, Bear EJ. The principles of directed cell migration. *Nat Rev Mol Cell Biol.* 2021;22(8):529–47. <https://doi.org/10.1038/s41580-021-00366-6>
- Mathieu M, Isomursu A, Ivaska J. Positive and negative durotaxis—mechanisms and emerging concepts. *J Cell Sci.* 2024;137(8):jcs261919. <https://doi.org/10.1242/jcs.261919>
- Janmey AP, Fletcher AD, Reinhart-King AC. Stiffness sensing by cells. *Physiol Rev.* 2020;100(2):695–724. <https://doi.org/10.1152/physrev.00013.2019>
- Discher DE, Janmey P, Wang Y-L. Tissue cells feel and respond to the stiffness of their substrate. *Science.* 2005;310(5751):1139–43. <https://doi.org/10.1126/science.1116995>
- Engler AJ, Richert L, Wong JY, Picart C, Discher DE. Surface probe measurements of the elasticity of sectioned tissue, thin gels and polyelectrolyte multilayer films: correlations between substrate stiffness and cell adhesion. *Surf Sci.* 2004;570(1–2):142–54. <https://doi.org/10.1016/j.susc.2004.06.179>
- Li Z, Dranoff JA, Chan EP, Uemura M, Sévigny J, Wells RG. Transforming growth factor- $\beta$  and substrate stiffness regulate portal fibroblast activation in culture. *Hepatology.* 2007;46(4):1246–56. <https://doi.org/10.1002/hep.21792>
- Sergey PV, Ana PM, Sabass B, Clare WM. Force fluctuations within focal adhesions mediate ECM-rigidity sensing to guide directed cell migration. *Cell.* 2012;151(7):1513–27. <https://doi.org/10.1016/j.cell.2012.11.034>
- Geiger B, Spatz JP, Bershadsky AD. Environmental sensing through focal adhesions. *Nat Rev Mol Cell Biol.* 2009;10(1):21–33. <https://doi.org/10.1038/nrm2593>
- Parsons JT, Horwitz AR, Schwartz MA. Cell adhesion: integrating cytoskeletal dynamics and cellular tension. *Nat Rev Mol Cell Biol.* 2010;11(9):633–43. <https://doi.org/10.1038/nrm2957>
- Burridge K, Guilluy C. Focal adhesions, stress fibers and mechanical tension. *Exp Cell Res.* 2016;343(1):14–20. <https://doi.org/10.1016/j.yexcr.2015.10.029>
- Gupta M, Doss LB, Kocgozlu L, Pan M, Mège R-M, Callan-Jones A, et al. Cell shape and substrate stiffness drive actin-based cell polarity. *Phys Rev E.* 2019;99(1). <https://doi.org/10.1103/PhysRevE.99.012412>
- Prager-Khoutorsky M, Lichtenstein A, Krishnan R, Rajendran K, Mayo A, Kam Z, et al. Fibroblast polarization is a matrix-rigidity-dependent process controlled by focal adhesion mechanosensing. *Nat Cell Biol.* 2011;13(12):1457–65. <https://doi.org/10.1038/ncb2370>
- Young LE, Heimsath EG, Higgs HN. Cell type-dependent mechanisms for formin-mediated assembly of filopodia. *Mol Biol Cell.* 2015;26(25):4646–59. <https://doi.org/10.1091/mbc.e15-09-0626>
- Vaillant DC, Copeland SJ, Davis C, Thurston SF, Abdennur N, Copeland JW. Interaction of the N- and C-terminal autoregulatory domains of FRL2 does not inhibit FRL2 activity. *J Biol Chem.* 2008;283(48):33750–62.
- Kühn S, Erdmann C, Kage F, Block J, Schwenkmezger L, Steffen A, et al. The structure of FMNL2–Cdc42 yields insights into the mechanism of lamellipodia and filopodia formation. *Nat Commun.* 2015;6(1):7088. <https://doi.org/10.1038/ncomms8088>
- Dimchev V, Lahmann I, Koestler SA, Kage F, Dimchev G, Steffen A, et al. Induced Arp2/3 complex depletion increases FMNL2/3 formin expression and filopodia formation. *Front Cell Develop Biol.* 2021;9. <https://doi.org/10.3389/fcell.2021.634708>
- Fox S, Tran A, Trinkle-Mulcahy L, Copeland JW. Cooperative assembly of filopodia by the formin FMNL2 and I-BAR domain protein IRTKS. *J Biol Chem.* 2022;298(11):102512. <https://doi.org/10.1016/j.jbc.2022.102512>
- Péladeau C, Heibein A, Maltez MT, Copeland SJ, Copeland JW. A specific FMNL2 isoform is up-regulated in invasive cells. *BMC Cell Biol.* 2016;17(1). <https://doi.org/10.1186/s12860-016-0110-z>
- Gardberg M, Heuser VD, Koskivuo I, Koivisto M, Carpén O. FMNL2/FMNL3 formins are linked with oncogenic pathways and predict melanoma outcome. *J Pathol Clin Res.* 2016;2(1):41–52. <https://doi.org/10.1002/cjp2.34>
- Zhu X-L, Liang L, Ding Y-Q. Overexpression of FMNL2 is closely related to metastasis of colorectal cancer. *Int J Colorectal Dis.* 2008;23(11):1041–47. <https://doi.org/10.1007/s00384-008-0520-2>
- Zhu XL, Zeng YF, Guan J, Li YF, Deng YJ, Bian XW, et al. FMNL2 is a positive regulator of cell motility and metastasis in colorectal carcinoma. *J Pathol.* 2011;224(3):377–88. <https://doi.org/10.1002/path.2871>
- Block J, Breitsprecher D, Kühn S, Winterhoff M, Kage F, Geffers R, et al. FMNL2 drives actin-based protrusion and migration downstream of Cdc42. *Curr Biol.* 2012;22(11):1005–12. <https://doi.org/10.1016/j.cub.2012.03.064>
- Kage F, Winterhoff M, Dimchev V, Mueller J, Thalheim T, Freise A, et al. FMNL formins boost lamellipodial force generation. *Nat Commun.* 2017;8(1):14832. <https://doi.org/10.1038/ncomms14832>
- Grikscheit K, Frank T, Wang Y, Grosse R. Junctional actin assembly is mediated by Formin-like 2 downstream of Rac1. *J Cell Biol.* 2015;209(3):367–76. <https://doi.org/10.1083/jcb.201412015>
- Wang Y, Arjonen A, Pouwels J, Ta H, Pausch P, Bange G, et al. Formin-like 2 promotes  $\beta$ 1-integrin trafficking and invasive motility downstream of PKC $\alpha$ . *Dev Cell.* 2015;34(4):475–83. <https://doi.org/10.1016/j.devcel.2015.06.015>
- Huang Y, Su J, Liu J, Yi X, Zhou F, Zhang J, et al. YAP activation in promoting negative durotaxis and acral melanoma progression. *Cells [Internet].* 2022;11(22). <https://doi.org/10.3390/cells11223543>
- Isomursu A, Park K-Y, Hou J, Cheng B, Mathieu M, Shamsan GA, et al. Directed cell migration towards softer environments. *Nat Mater.* 2022;21(9):1081–90. <https://doi.org/10.1038/s41563-022-01294-2>
- Kitzing TM, Wang Y, Pertz O, Copeland JW, Grosse R. Formin-like 2 drives amoeboid invasive cell motility downstream of RhoC. *Oncogene.* 2010;29(16):2441–48. <https://doi.org/10.1038/ncr.2009.515>
- Chesarone MA, DuPage AG, Goode BL. Unleashing formins to remodel the actin and microtubule cytoskeletons. *Nat Rev Mol Cell Biol.* 2010;11(1):62–74. <https://doi.org/10.1038/nrm2816>
- Colón-Franco JM, Gomez TS, Billadeau DD. Dynamic remodeling of the actin cytoskeleton by FMNL1y is required for structural maintenance of the Golgi complex. *J Cell Sci.* 2011;124(18):3118–26. <https://doi.org/10.1242/jcs.083725>

31. Lorenzen L, Frank D, Schwan C, Grosse R. Spatiotemporal regulation of FMNL2 by N-terminal myristoylation and C-terminal phosphorylation drives rapid filopodia formation. *Biomolecules*. 2023;13(3). <https://doi.org/10.3390/biom13030548>.
32. Horton ER, Byron A, Askari JA, Dhj N, Millon-Frémillon A, Robertson J, et al. Definition of a consensus integrin adhesome and its dynamics during adhesion complex assembly and disassembly. *Nat Cell Biol*. 2015;17(12):1577–87. <https://doi.org/10.1038/ncb3257>.
33. Horton ER, Astudillo P, Humphries MJ, Humphries JD. Mechanosensitivity of integrin adhesion complexes: role of the consensus adhesome. *Exp Cell Res*. 2016;343(1):7–13. <https://doi.org/10.1016/j.yexcr.2015.10.025>.
34. Hakeem RM, Subramanian BC, Hockenberry MA, King ZT, Butler MT, Legant WR, et al. A photopolymerized hydrogel system with dual stiffness gradients reveals distinct actomyosin-based mechano-responses in fibroblast durotaxis. *ACS Nano*. 2023;17(1):197–211. <https://doi.org/10.1021/acsnano.2c05941>.
35. Schliwa M, van Blerkom J. Structural interaction of cytoskeletal components. *J Cell Biol*. 1981;90(1):222–35. <https://doi.org/10.1083/jcb.90.1.222>.
36. Marcotti S, Belo de Freitas D, Troughton LD, Kenny FN, Shaw TJ, Stramer BM, et al. A workflow for rapid unbiased quantification of fibrillar feature alignment in biological images. *Front Comp Sci*. 2021;3. <https://doi.org/10.3389/fcomp.2021.745831>.
37. de Gennes PG, Prost J. The physics of liquid crystals. Clarendon Press; 1993. <https://doi.org/10.1063/1.2808028>.

### Publisher's Note

Springer Nature remains neutral with regard to jurisdictional claims in published maps and institutional affiliations.